Journal of Southeast University (English Edition) Vol. 24, No. 4, pp. 487 – 491 Dec. 2008 ISSN 1003—7985

Quadrature error and offset error suppression circuitry for silicon micro-gyroscope

Yang Bo Zhou Bailing Wang Shourong

(School of Instrument Science and Engineering, Southeast University, Nanjing 210096, China)

Abstract: The reasons for inducing quadrature error and offset error are analyzed and the expressions of quadrature error and offset error are induced. The open-loop system analysis indicates that, in order to avoid the appearance of harmonic peaks, the frequency difference δ_f between drive mode and sense mode must be less than $1/(2Q_y)$. In order to eliminate the effects of the quadrature error and the offset error, as well as the inherent non-linearity in the capacitance-type sensors, a closed-loop feedback control circuit with quadrature correction is designed. The experimental results indicate that the quadrature error and offset error are corrected. By comparing with open-loop detection, the closed-loop feedback control circuit with quadrature correction decreases the non-linearity of the scale factor from 16.02% to 0.35%, widens the maximum rate capability from ±270 (°)/s to ± 370 (°)/s and increases the stability of zero bias from 155.2 (°)/h to 60.6 (°)/h.

Key words: silicon micro-gyroscope (SMG); quadrature error; offset error; closed-loop feedback; stability of zero bias

The silicon micro-gyroscope (SMG) is an important MEMS inertia sensor with a broad application in national economy and defense fields[1-3]. Due to restrictive tolerance in the process, structural imperfections that reduce performance of fabricated SMGs are typical and induce the structural error of the SMG[4-5]. While it has a zero input of rotation rate, the output of the preamplifier still comprises an offset error, which is an in-phase or out-phase component with a Coriolis signal, and a quadrature error, which is a quadrature component with a Coriolis signal[6]. There are many reasons that cause the mechanical coupling, such as asymmetry and anisoelasticity of structure, unbalance of stress on the support beams, different quality factors, asymmetry in the aerodynamic drag and structural damping. The quadrature error and the offset error limit the AC gain in front of the demodulator, give rise to sensitivity to phase variation and result in poor bias stability. The quadrature error and the offset error were reduced by optimizing the structure of the SMG, such as decoupling the drive mode and sense mode, improving support beams and so on. But these methods cannot completely reduce but only partially reduce the quadrature error and the offset error, and sometimes without effect[6-8]. So the reasons for inducing the quadrature error and the offset error are analyzed and a closed-loop feedback control circuit with quadrature correction is designed to suppress the quadrature error and the offset error.

Received 2008-03-20.

Biography: Yang Bo (1979—), male, doctor, lecturer, yangbo20022002@163.com.

Citation: Yang Bo, Zhou Bailing, Wang Shourong. Quadrature error and offset error suppression circuitry for silicon micro-gyroscope[J]. Journal of Southeast University (English Edition), 2008, 24(4): 487 – 491.

1 Analysis of Structure Error

The structure and model of the SMG are shown in Fig. 1. To measure rotation rate, the frame (including the inner frame and outer frame) are driven at a fixed amplitude along the x-axis by applying an electrostatic drive force to the frame along the x-axis. In the absence of rotation, there is no motion of the inner frame along the y-axis under ideal conditions. As a rule, fabrication tolerance contributes to imperfections in the micro-gyroscope.

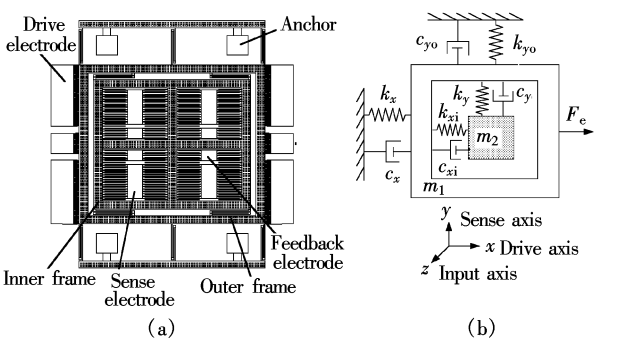

Fig. 1 The structure and model of SMG. (a) The structure of SMG; (b) The model of SMG

Fig. 2 is the schematic of mechanical movement error. According to the layout of the differential sense electrode of the SMG, the extraction method of the Coriolis signal can suppress the rotary movement error, but the translation movement error (quadrature error and offset error) as well as the Coriolis signal is amplified, so the closed-loop feedback control circuit with quadrature correction is used mainly to rectify the translation movement error. Fabrication imperfections are major factors resulting in quadrature errors and offset errors. In practice, imperfections are reflected in asymmetry and anisoelasticity of the structure, and can be captured as a mis-alignment of the principal axis of the elasticity from the intended axis of the symmetry of the structure[7-8].

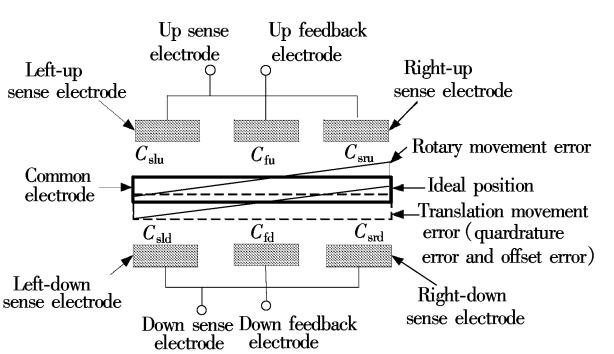

Fig. 2 Schematic of mechanical movement error

Fig. 3 shows the anisoelasticity of the SMG in the outer frame and the inner frame. Stiffness matrices in the outer frame and the inner frame are

$$k_{\mathrm{o}}=\begin{bmatrix}k_{x\mathrm{xo}} & k_{x\mathrm{yo}}\\ k_{y\mathrm{xo}} & k_{y\mathrm{yo}}\end{bmatrix},\quad k_{\mathrm{i}}=\begin{bmatrix}k_{x\mathrm{xi}} & k_{x\mathrm{yi}}\\ k_{y\mathrm{xi}} & k_{y\mathrm{yi}}\end{bmatrix} \tag{1}$$

where $k_{\mathrm{yo}}\gg k_x$, $k_{\mathrm{xi}}\gg k_y$ and

$$k_{x\mathrm{xo}}=\frac{k_x+k_{\mathrm{yo}}}{2}+\frac{k_x-k_{\mathrm{yo}}}{2}\cos(2\varepsilon_1)\approx k_x$$

$$k_{x\mathrm{yo}}=K_{y\mathrm{xo}}=\frac{k_{\mathrm{yo}}-k_x}{2}\sin(2\varepsilon_1)\approx k_{\mathrm{yo}}\varepsilon_1$$

$$k_{y\mathrm{yo}}=\frac{k_x+k_{\mathrm{yo}}}{2}+\frac{k_{\mathrm{yo}}-k_x}{2}\cos(2\varepsilon_1)\approx k_{\mathrm{yo}}$$

$$k_{x\mathrm{xi}}=\frac{k_{\mathrm{xi}}+k_y}{2}+\frac{k_{\mathrm{xi}}-k_y}{2}\cos(2\varepsilon_2)\approx k_{\mathrm{xi}}$$

$$k_{x\mathrm{yi}}=k_{y\mathrm{xi}}=\frac{k_y-k_{\mathrm{xi}}}{2}\sin(2\varepsilon_2)\approx -k_{\mathrm{xi}}\varepsilon_2$$

$$k_{y\mathrm{yi}}=\frac{k_{\mathrm{xi}}+k_y}{2}+\frac{k_y-k_{\mathrm{xi}}}{2}\cos(2\varepsilon_2)\approx k_y$$

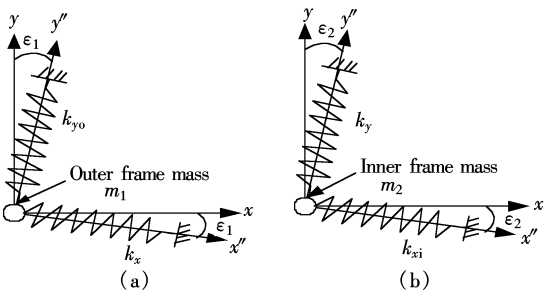

Fig. 3 The anisoelasticity of the SMG in the outer frame and the inner frame. (a) The principal axis of elasticity of the outer frame rotates at a small angle; (b) The principal axis of elasticity of the inner frame rotates at a small angle

Because of the anisoelasticity in the outer frame and the inner frame, the coupling elastic forces in the sensing direction are

$$F_{x\mathrm{yo}}=k_{x\mathrm{yo}}x_{\mathrm{o}}=k_{x\mathrm{yo}}x_{\mathrm{d}}=k_{\mathrm{yo}}\varepsilon_1 x_{\mathrm{o}} \tag{2}$$

$$F_{x\mathrm{yi}}=k_{x\mathrm{yi}}(x_{\mathrm{i}}-x_{\mathrm{o}})=-k_{\mathrm{xi}}\varepsilon_2(x_{\mathrm{i}}-x_{\mathrm{o}}) \tag{3}$$

where x_{o}, x_{i} are the drive displacements of the outer frame and the inner frame in x direction, respectively.

Fig. 4 is the scheme of the coupling elastic force applied to the outer frame and the inner frame [6].

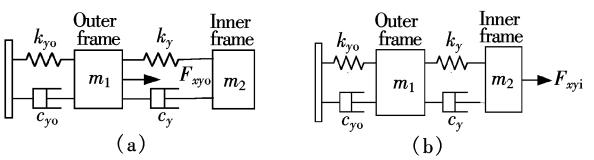

Fig. 4 The scheme of the coupling elastic force applied to the outer frame and the inner frame. (a) The coupling elastic force is applied to the outer frame; (b) The coupling elastic force is applied to the inner frame

So the motion equations are

$$m_2\ddot{y}_{\mathrm{i1}}+c_y(\dot{y}_{\mathrm{i1}}-\dot{y}_{\mathrm{o1}})+k_y(y_{\mathrm{i1}}-y_{\mathrm{o1}})=0 \tag{4}$$

$$m_1\ddot{y}_{\mathrm{o1}}+c_{\mathrm{yo}}\dot{y}_{\mathrm{o1}}+k_{\mathrm{yo}}y_{\mathrm{o1}}+c_y(\dot{y}_{\mathrm{o1}}-y_{\mathrm{i1}})+k_y(y_{\mathrm{o1}}-y_{\mathrm{i1}})=F_{x\mathrm{yo}} \tag{5}$$

$$m_2\ddot{y}_{\mathrm{i2}}+c_y(\dot{y}_{\mathrm{i2}}-\dot{y}_{\mathrm{o2}})+k_y(y_{\mathrm{i2}}-y_{\mathrm{o2}})=F_{x\mathrm{yi}} \tag{6}$$

$$m_1\ddot{y}_{\mathrm{o2}}+c_{\mathrm{yo}}\dot{y}_{\mathrm{o2}}+k_{\mathrm{yo}}y_{\mathrm{o2}}+c_y(\dot{y}_{\mathrm{o2}}-y_{\mathrm{i2}})+k_y(y_{\mathrm{o2}}-y_{\mathrm{i2}})=0 \tag{7}$$

where y_{o1}, y_{o2}, y_{i1}, y_{i2} are the displacements of the outer frame and the inner frame in y direction, respectively. The coupling displacements are

$$\left|\frac{y_{\mathrm{i1}}}{y_{\mathrm{s}}}\right|\approx\left|\frac{\omega_y^2\varepsilon_1}{2\Omega\omega_{\mathrm{d}}}\left(\mathrm{j}-\frac{\eta_2}{Q_y}\right)\right| \tag{8}$$

$$\left|\frac{y_{\mathrm{i2}}}{y_{\mathrm{s}}}\right|\approx\left|\frac{\omega_{\mathrm{d}}\varepsilon_2\mathrm{j}}{2\Omega}\right| \tag{9}$$

where y_{s} is the sense displacement due to the input of rotation rate; $\omega_y=(k_y/m_2)^{1/2}$, $\omega_{\mathrm{d}}=(k_x/(m_1+m_2))^{1/2}$, $Q_y=m_2\omega_y/c_y$, $\eta_2=\omega_{\mathrm{d}}/\omega_y$; Ω is the input rotational rate along the z-axis.

As in the stiffness case, asymmetric damping can arise, which is principally caused by different quality factors or asymmetry in aerodynamic drag, structural damping, etc., in the two axes. Similar to the stiffness case, when the principal axis of damping of the outer frame and the inner frame rotates at a small angle separately, the coupling displacements are

$$\left|\frac{y_{\mathrm{i3}}}{y_{\mathrm{s}}}\right|\approx\left|\frac{\omega_y^2(c_{\mathrm{yo}}-c_x)\mu_1}{-2k_{\mathrm{yo}}\Omega}\left(\frac{\eta_2\mathrm{j}}{Q_y}+1\right)\right| \tag{10}$$

$$\left|\frac{y_{\mathrm{i4}}}{y_{\mathrm{s}}}\right|\approx\left|\frac{(c_y-c_{\mathrm{xi}})\mu_2\omega_{\mathrm{d}}^2}{-2k_{\mathrm{xi}}\Omega}\right| \tag{11}$$

where y_{i3} and y_{i4} are the coupling displacements of the inner frame in y direction because of the principal axis of the damping of the outer frame and the inner frame rotating at small angles u_1 and u_2, respectively.

In the worst condition, the quadrature error and offset error are

$$\left|\frac{y_{\mathrm{q}}}{y_{\mathrm{s}}}\right|\approx\frac{\Omega_{\mathrm{qua}}}{\Omega}=\frac{\left|\frac{\omega_y^2\varepsilon_1}{2\omega_{\mathrm{d}}}\right|+\left|\frac{\omega_{\mathrm{d}}\varepsilon_2}{2}\right|+\left|\frac{\omega_{\mathrm{d}}\omega_y(c_{\mathrm{yo}}-c_x)\mu_1}{2k_{\mathrm{yo}}Q_y}\right|}{\Omega} \tag{12}$$

$$\left|\frac{y_{\mathrm{o}}}{y_{\mathrm{s}}}\right|\approx\frac{\Omega_{\mathrm{off}}}{\Omega}=\frac{\left|\frac{\omega_y\varepsilon_1}{2Q_y}\right|+\left|\frac{\omega_y^2(c_{\mathrm{yo}}-c_x)\mu_1}{2k_{\mathrm{yo}}}\right|+\left|\frac{(c_y-c_{\mathrm{xi}})\mu_2\omega_{\mathrm{d}}^2}{2k_{\mathrm{xi}}}\right|}{\Omega} \tag{13}$$

where y_{q} is the total quadrature error and y_{o} is the total offset error, Ω_{qua} is the equivalent rotational rate of the quadrature error, and Ω_{off} is the equivalent rotational rate of the offset error.

2 Open-Loop Detection of Quadrature Error and Offset Error

In order to compensate for the quadrature error and offset error, the quadrature error and the offset error must be detected first. Because they have the same frequency as the sense signal, we adopt the phase sensitive demodulator to separate these error signals from the sense signal. Fig. 5 is the schematic of open-loop detection. The output voltage $u(t)$ is

$$U(s) = A_x\omega_d K_{open} G(s,\omega_d) F(s) \Omega(s) + K_{open} N_y(s,\omega_d) F(s) \tag{14}$$

where A_x is the oscillating amplitude of the drive mode, $F(s)$ is the low pass filter, $G(s,\omega_d) = e^{j\phi_{op}} G(s - j\omega_d) + e^{-j\phi_{op}} G(s + j\omega_d)$, $G(s)$ is the transfer function of the sense mode,

$$N_y(s,\omega_d) = e^{j\phi_{op}} N_y(s - j\omega_d) + e^{-j\phi_{op}} N_y(s + j\omega_d)$$

The transfer function of the open-loop system is

$$H_{open}(s) = \frac{U(s)}{\Omega(s)} = A_x\omega_d K_{open} G(s,\omega_d) F(s) = 2A_x\omega_d K_{open} F(s) \cdot \frac{\cos\phi_{op}\left[s^2 + \frac{\omega_y}{Q_y}s + \omega_y^2 - \omega_d^2\right] - \sin\phi_{op}\omega_d\left[2s + \frac{\omega_y}{Q_y}\right]}{(s - a_p - j\omega_d)(s - b_p - j\omega_d)(s - a_p + j\omega_d)(s - b_p + j\omega_d)} \tag{15}$$

where a_p, b_p are the poles of $G(s)$.

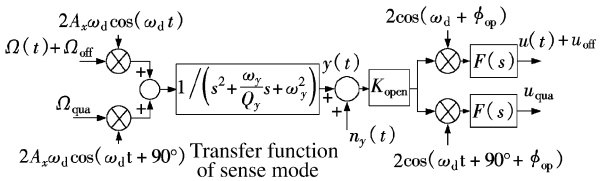

Fig. 5 Schematic of open-loop detection

Fig. 6 shows the open-loop amplitude and phase curves in different quality factors when $(\omega_y - \omega_d)/(2\pi) = 100$ Hz. And the low loop filter $F(s)$ is not taken into account. It is evident that, when the quality factor Q_y adds up to a certain value, the open-loop amplitude curve will show the harmonic peak. As a result, the bigger the quality factor Q_y, the sharper the harmonic peak. In order to suppress the harmonic peak, we have to design a few high-order low pass filters in subsequent circuits and the band width of the low pass filters must be smaller than those in the preceding system, which, as a result, will increase the complexity of circuit, worsen the system performance and shrink the system band width. So the relative frequency difference δ_f and quality factor Q_y must match each other.

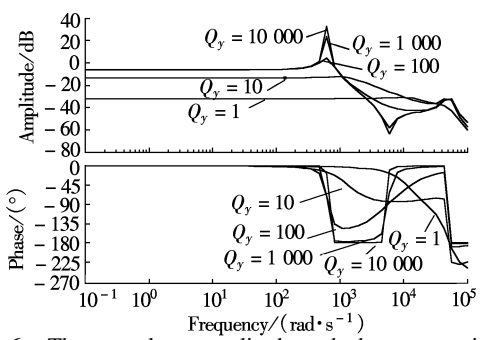

Fig. 6 The open-loop amplitude and phase curve in different quality factors Q_y

The band width of input rotational velocity is narrow. When $Q_y \gg 1$, in the low-frequency scale, due to $j(\omega_y(1 - 1/(4Q_y^2))^{0.5} + \omega_d) \gg j\omega$, the multiplier of denominator $(s - a_p - j\omega_d)$ and $(s - b_p + j\omega_d)$ in Eq. (15) can be simplified into $(-a_p - j\omega_d)$ and $(-b_p + j\omega_d)$, so Eq. (15) can be simplified into

$$H_{open}(s) \approx \frac{2A_x\omega_d K_{open} F(s)}{(\omega_y + \omega_d)^2} \cdot \frac{\cos\phi_{op}(s^2 + s\omega_y/Q_y + \omega_y^2 - \omega_d^2) - \sin\phi_{op}\omega_d(2s + \omega_y/Q_y)}{s^2 + s\omega_y/Q_y + (\omega_y - \omega_d)^2} \tag{16}$$

Without consideration of the low pass filter $F(s)$, the preceding system can be simplified as a second-order dynamic system. The equivalent quality factor is

$$Q_{eq,y} = \delta_f Q_y$$

In order to avoid the appearance of a harmonic peak, the system must be designed as an over-damping or critical-damping system; that is, the value of equivalent quality factor must be limited below 0.5, i.e.,

$$Q_{eq,y} = \delta_f Q_y \leqslant \frac{1}{2}$$

i.e.

$$\delta_f \leqslant \frac{1}{2Q_y} \tag{17}$$

It indicates that, in order to avoid the appearance of a harmonic peak, the bigger the quality factor Q_y is, the smaller the relative frequency difference δ_f is. That is why the JPL's (Jet Propulsion Laboratory) MEMS gyroscope which has a very big quality factor must match precisely the frequency between drive mode and sense mode[9].

3 Quadrature Error and Offset Error Rectification

The quadrature error and offset error which are much bigger than the sense signal aggravate non-linearity between the input rotation rate and output voltage, give rise to the sensitivity to phase variation, and result in poor bias stability. In order to improve the performance of the SMG, the quadrature error and offset error must be corrected. Fig. 7 is the schematic of the closed-loop feedback control circuit with quadrature correction. The quadrature error is amended by the branch circuit of the quadrature correction and the offset error is amended by the branch circuit of the offset correction. Fig. 8 is a simplified schematic of the quadrature feedback control, where K_{for} is the coefficient of the force function and $K_{qua} = 0.5U_{car}U_{dem}K_{int}K_{ac}A_x\omega_d$.

The transfer function of the quadrature feedback control is

$$H_{qua}(s) = \frac{G(s,\omega_d) K_{qua} F_{qua}(s)(K_p + K_i/s + K_d s)}{1 + G(s,\omega_d) K_{qua} F_{qua}(s)(K_p + K_i/s + K_d s) K_{for}/(A_x\omega_d)} \tag{18}$$

Because the quadrature feedback control is the Ⅰ-system, the steady-state error is zero and

$$H_{qua}(s)\,|_{s=0} = \frac{A_x\omega_d}{K_{for}} \tag{19}$$

Fig. 9 is the Nyquist curve of the open-loop quadrature correction. We can see from Fig. 10 that, when the frequen-

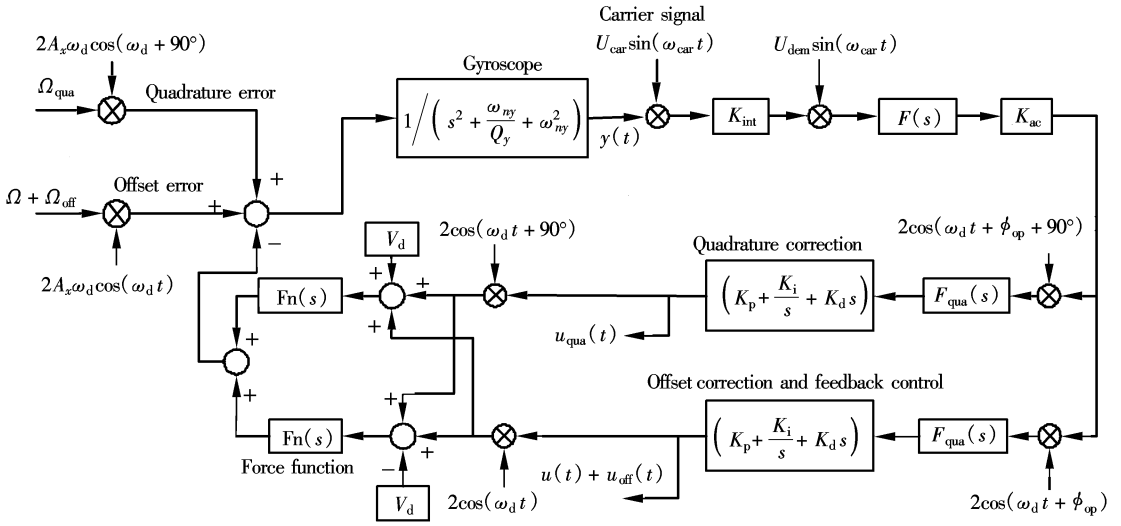

Fig. 7 Schematic of the closed-loop feedback control circuit with quadrature correction

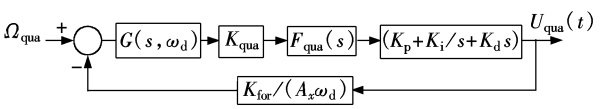

Fig. 8 Simplified schematic of the quadrature feedback control

cy varies from 0^+ Hz to $+\infty$ Hz, the Nyquist curve does not encircle the criterion point $(-1,0)$ and all of the poles of the open-loop transfer function are located on the left of the imaginary axis, which means that the quadrature feedback control system is steady.

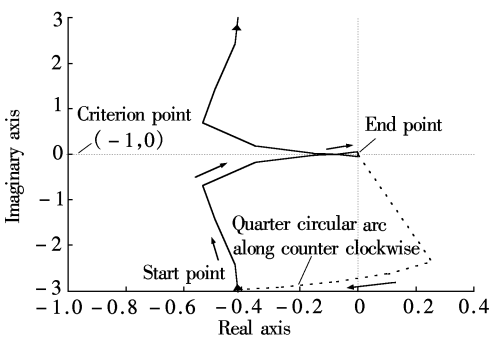

Fig. 9 The Nyquist curve of the open-loop quadrature correction

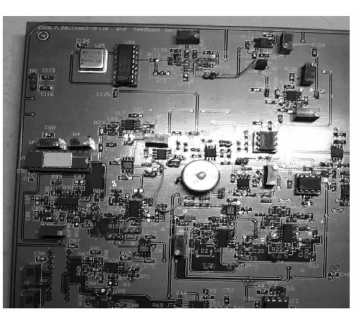

Fig. 10 The PCB circuitry of the closed-loop feedback control with quadrature correction

4 Experimental Results and Discussion

Fig. 10 is the PCB circuitry of the closed-loop feedback control with quadrature correction. Fig. 11 shows the effect of the closed-loop feedback control circuit with quadrature correction. It is evident that the quadrature error and offset error are eliminated by the closed-loop feedback control circuit with quadrature correction. Fig. 12 and Fig. 13 present the experimental results. Compared with open-loop detection, the closed-loop feedback control circuit with quadrature correction decreases the non-linearity of the scale factor from 16.02% to 0.35%, widens the maximum rate capability from ±270 (°)/s to ± 370 (°)/s and increases the stability of zero bias from 155.2 (°)/h to 60.6 (°)/h.

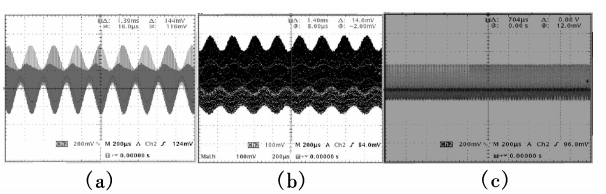

Fig. 11 The effect of the closed-loop feedback control circuit with quadrature correction. (a) Output wave of preamplifier at open-loop detection; (b) Output wave of preamplifier at quadrature correction; (c) Output wave of preamplifier at the closed-loop feedback control with quadrature correction

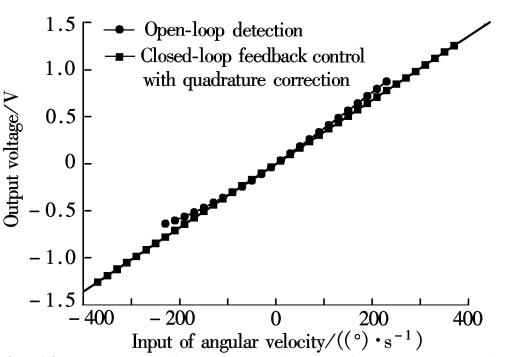

Fig. 12 Output of SMG vs. input of angular velocity

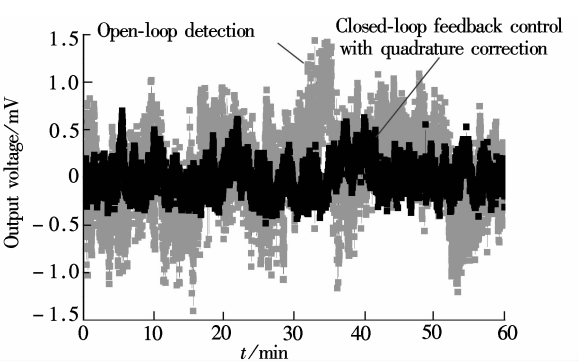

Fig. 13 Output of SMG at zero input

References

[1] Geen John A. Very low cost gyroscopes[J]. *Sensors*, 2005, **37**(3): 537 - 540.

[2] Dixon Richard H, Bouchaud Jérémie. Markets and applications for MEMS inertial sensors[C]//*Proceedings of SPIE*, *MEMS/MOEMS Components and Their Applications* Ⅲ. San Jose, 2006, **6113**: 611306.

[3] Barbour Neil, Schmidt George. Inertial sensor technology trends[J]. *IEEE Sensors Journal*, 2001, **1**(4): 332 - 339.

[4] Shkel A, Howe R. Dynamic and control of micromachined gyroscope[C]//1999 *American Control Conference*. San Diego, 1999: 2119 - 2124.

[5] Braxmaierl M, GaiBerl A, Link T. Cross-coupling of the oscillation modes of vibratory gyroscopes[C]//*The* 12*th International Conference on Solid State Sensors*, *Actuators and Microsystem*. Boston, 2003: 167 - 170.

[6] Iyer Sitaraman V. Modeling and simulation of non-idealities in a *z*-axis CMOS-MEMS gyroscope[D]. Pittsburgh: Carnegie Mellon University, 2003.

[7] Alper Said Emre, Akin Tayfun. Symmetrical and decoupled nickel microgyroscope on insulating substrate[J]. *Sensors and Actuators A*, 2004, **115**((2/3): 336 - 350.

[8] Geiger W, Butt W U, Gaiber A, et al. Decouple microgyros and the design principle daver[J]. *Sensors and Actuators A*, 2004, **95**(2/3): 239 - 249.

[9] Kim D J, M'Closkey R T. Real-time tuning of MEMS gyro dynamics[C]//2005 *American Control Conference*. Portland, 2005: 3598 - 3603.

硅微陀螺仪正交误差和失调误差抑制线路

杨 波 周百令 王寿荣

(东南大学仪器科学与工程学院,南京 210096)

摘要:分析了正交误差和失调误差产生的原因,推导了正交误差和失调误差的表达式. 开环系统分析表明,为了避免开环系统出现谐振峰,两模态(驱动模态与敏感模态)频差 δ_f 必须小于 $1/(2Q_y)$. 为了消除正交误差、失调误差及电容传感器自身非线性的影响,设计了一个可实现正交误差校正的闭环反馈电路. 实验结果表明,正交误差和失调误差得到较好抑制. 与开环检测相比,闭环反馈回路将标度因数非线性从 16.02% 减少到 0.35%,将最大测量范围从 ±270(°)/s 扩展到 ± 370(°)/s,将零偏稳定性从 155.2(°)/h 提高到 60.6(°)/h.

关键词:硅微陀螺仪;正交误差;失调误差;闭环反馈;零偏稳定性

中图分类号:U666.123